Chapter 4

Iron doped titania/ Polyaniline composite: an efficient electrocatalyst for hydrogen evolution reaction in acidic medium

.

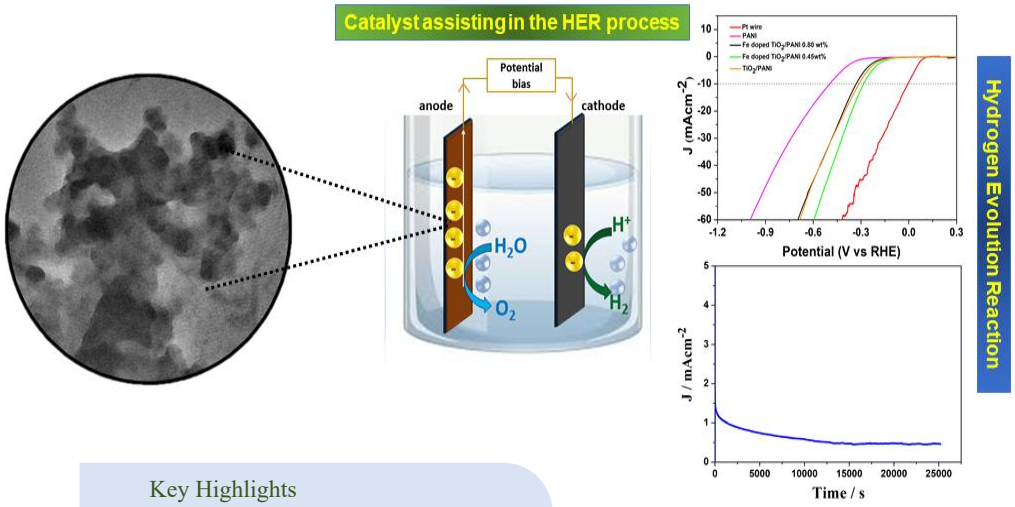

Key Highlights

- In-situ polymerization method was used as synthesis procedure.
- 285 mV overpotential was required
- The catalyst is quite stable in 0.5 M H_2SO_4 up to 8 hr
- Optimum catalytic activity was obtained with 0.45 wt% of PANI

4.1 Introduction

Among the alternate fuel sources, hydrogen has the viability to replace fossil fuels. Although non-noble metal (Ni, Co, Mo, Fe) sulfides, phosphides, selenides and some other porous materials including conductive metal-organic framework and other doped carbon materials are proved to be the best choice for efficient HER, apart from oxide-based catalysts almost all of them involves complex synthesis procedure and hazardous chemical use. TiO_2 is an attractive material in terms of its processing cost, abundance, low toxicity, its corrosion resistivity, and environmental friendliness. However, due to poor conductivity TiO_2 has been less studied as an electrocatalyst. Later it was found that conductivity of TiO_2 can be enhanced by doping, creating oxygen vacancy, etc [1,2]. The band gap of TiO_2 can be shortened by doping which ultimately improves the electrical properties. The metal-support interactions can also be enhanced by doping, leading to increased electrocatalytic performance [3,4]. Among the anatase and rutile phases of titania, anatase phase due to being an indirect band gap material offers a better charge carrier lifetime. Moreover, the pure anatase phase delivers high surface area and pore volume which leads to better adsorption of reactant molecules to carry out electrocatalytic reactions [5]. As we have mentioned in Chapter 3 Fe doped TiO_2 proved to be efficient towards HER in alkaline medium. But due to low corrosion resistive property of 3d transition metals they are less studied towards HER in acidic medium.

The flaws of TiO_2 and Fe nanoparticles regarding lower electrical conductivity and corrosion in acidic medium are conventionally overwhelmed by using nanostructured carbon materials (like graphene, amorphous carbon, and multiwalled carbon nanotubes (MWCNTs) [6]. However, the use of Polyaniline (PANI) is not as much discussed in this aspect as the carbon-based materials although PANI has been regarded as one of the promising candidates for electrocatalytic reactions, and

---

This part of the thesis is published in:

Lahkar, S., Brahma, R., and Dolui, S.K. Iron Doped Titania/Polyaniline Composite: An Efficient Electrocatalyst for Hydrogen Evolution Reaction in Acidic Medium. *Catalysis Research*, *3*(1):1-18, 2023.

supercapacitor because of its excellent chemical stability, high conductivity, strong adsorption capability of reactants, and also corrosion resistivity towards active metal elements [7,8]. Hence, in our present study, we synthesized a PANI-based composite for HER. But regardless of the mentioned unique properties of PANI, HER doesn't benefit much from PANI alone because of its inadequate hydrogen adsorption energy. Current research has focused on the optimization of the catalytic activity by enhancing the interfacial coupling between the support and active components to finely tune their band levels as well as the active sites [9,10]. Here, we tried to increase the catalytic activity of PANI towards HER by interfacial electronic coupling with Fe doped TiO_2. The composite Fe doped TiO_2@PANI has been synthesized by a simple and green insitu polymerization method. The physical properties of the catalyst are investigated by XRD, FTIR, SEM, and TEM. The electrochemical performance of the electrocatalyst is evaluated by studying its LSV curve and Tafel plot. Conductivity of the catalyst is assessed by EIS analysis. The plausible mechanism of HER is also discussed.

4.2 Materials and Methods

4.2.1 Materials Used

All the chemicals including titanium tetraisopropoxide (TTIP), Iron (III) nitrate nonahydrate ($Fe(NO_3)_3.9H_2O$), Methanol (CH_3OH), Ammonium peroxodisulfate ($(NH_4)2S_2O_8$), Hydrogen peroxide (H_2O_2), Aniline ($C_6H_5NH_2$), Acetic acid (CH_3COOH), Nafion and Sulphuric acid (H_2SO_4) purchased from Sigma-Aldrich are of analytical reagent grade purity and were used as received.

4.2.2 Methods

4.2.2.1 Synthesis of Fe doped TiO_2

Fe doped TiO_2 nanoparticles were synthesized by using the typical co-precipitation method [11] similarly described by Patle *et al.* 1M TTIP (solution 'A') and 0.05 M ferric nitrate (solution 'B') into distilled water were prepared separately with constant stirring for ½ hour. Subsequently, solution B was mixed with solution A and the solution mixture was kept for vigorous stirring for 2 hours. The precipitate

was then filtered and washed with water several times. Thus, obtained precipitate was mixed with 20ml H_2O_2 to get a clear solution with which a further 10mL distilled water was added until the colour changed from orange to yellow. The solution was left undisturbed for 2 days. After that the resulting sample was collected by filtering and washing with distilled water. As obtained sample was dried under vacuum and calcined for 6 hours at 500^0C.

4.2.2.2 Preparation of PANI and Fe doped TiO_2/PANI

PANI was synthesized by a conventional procedure where 1.75 mL of aniline monomer was mixed with 100 mL of the reaction solution [12]. The reaction solution was 0.4 M of acetic acid and 1 M methanol homogeneously mixed in 200 mL distilled water. Here ammonium persulphate (APS) served as the oxidant where 5.57 g APS was homogeneously mixed with 100 mL reaction solution separately. The temperature of both the solutions was brought down to 0-5^0C and quickly mixed under vigorous stirring for 30 sec. The mixture was aged for 10 hours maintaining the temperature within 0-5^0C. A dark green sample was obtained after filtration and wash which was dried in air for 24 hours to obtain PANI.

To synthesise Fe doped TiO_2/ PANI the oxidative polymerisation of aniline was carried out in presence of Fe doped TiO_2 nanoparticles. The above mentioned PANI synthesis procedure was repeated in presence 1.4 g of Fe doped TiO_2 particle dispersion in the reaction solution to obtain Fe doped TiO_2/PANI (0.45 wt%) nanocomposite. The process was repeated with 0.80 wt% PANI content and termed as Fe doped TiO_2/PANI (0.80 wt%) nanocomposite.

The notations, Fe doped TiO_2/PANI and Fe doped TiO_2@PANI have been used interchangeably throughout the paper. Also, Fe doped TiO_2/PANI signifies the PANI content of 0.45 wt%.

4.2.3 Electrochemical measurement:

The working electrode was prepared by dispersing 6 mg of the synthesized electrocatalyst in 0.1 mL of 0.5 wt% Nafion solution and coated onto the ~0.07 cm^2 surface area of the glassy carbon electrode (GCE, radius 1.5 mm) and then naturally

dried at room temperature. 0.5 M H_2SO_4 was the electrolyte for all the electrical measurements.

4.3 Results and Discussion

4.3.1 XRD analyses:

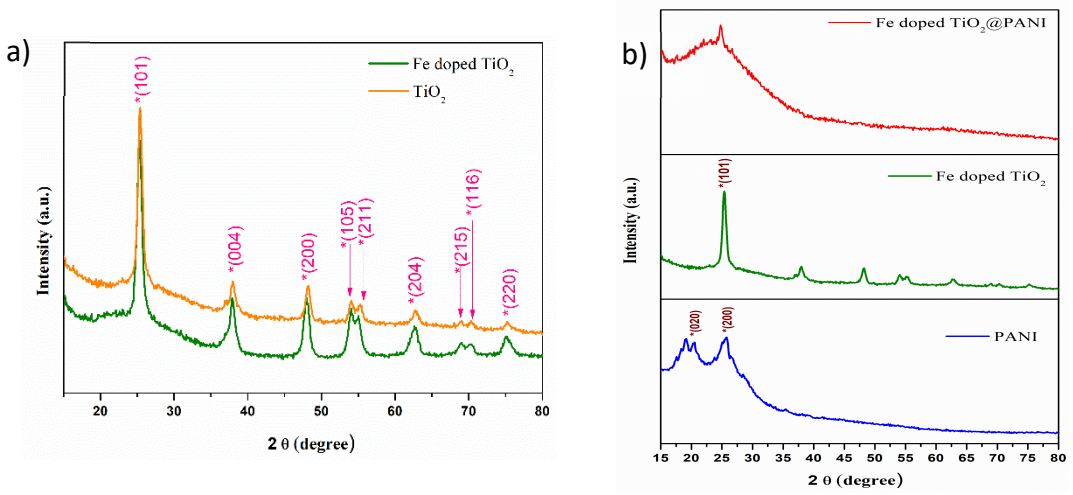

Figure 4.1 XRD pattern of (a) Comparison of Fe doped TiO_2 and TiO_2, (b) Fe doped TiO_2@PANI, Fe doped TiO_2 and PANI

Crystalline nature of the samples was examined by XRD. Hydrothermally synthesized TiO_2 nanoparticles show reflections at 2θ= 25.43°, 37.76°, 48.14°, 53.95°, 55.07°, 62.76°, 68.96°, 70.26°and 75.15° which belong to (101), (004), (200), (105), (211), (204), (116), (220) and (215) planes of titania [13], respectively in pure anatase phase (**Figure 4.1 (a)**). Comparison of the XRD graphs of TiO_2 and Fe doped TiO_2 led that after doping there occurred a little shift of the peaks to the lower angle. The shifting signifies the difference of radii of the lattice and dopant atom. However, absence of any peaks other than anatase phase in the XRD pattern confirms successful doping. In the obtained spectra of PANI (**Figure 4.1 (b)**), two prominent peaks are observed, one at 2θ = 20.4° for (020) plane and another at 2θ= 25.6° for (200) plane [14]. After incorporation of Fe doped TiO_2 into PANI a prominent peak was observed at 2θ= 25.43^0 due to the merging of (200) plane of PANI with (101) plane of TiO_2.

4.3.2 FTIR analyses:

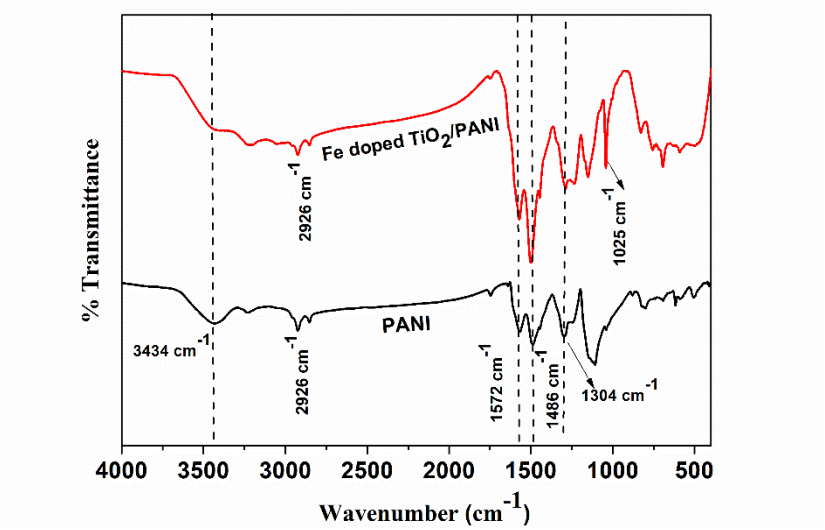

Figure 4.2 FTIR spectra of pure PANI and Fe doped TiO_2@PANI

The FTIR spectra of pure PANI and Fe doped TiO_2@PANI are shown in **Figure 4.2**. The broad peak at 3437 cm^{-1} in both PANI and Fe doped TiO_2@PANI is observed to be the N-H stretching vibration of amino group of polyanilines [15]. The peak at 2926 cm^{-1} is attributed to the C-H stretching frequency. For the C-N stretching frequency the peak observed is at 1304 cm^{-1} and the peak at 1572 cm^{-1} represents the benzoid ring. The C=C vibration of the aromatic ring indicating the polymer chain was observed at the peak 1486 cm^{-1}[16, 17, 18]. The spectrum of Fe doped TiO_2/PANI shows a significant absorption peak at ~1025 cm^{-1} due to Ti-O-C bond confirming the covalent linkage of Fe doped TiO_2 particle to the PANI [19].

4.3.3 Morphological and EDX analyses:

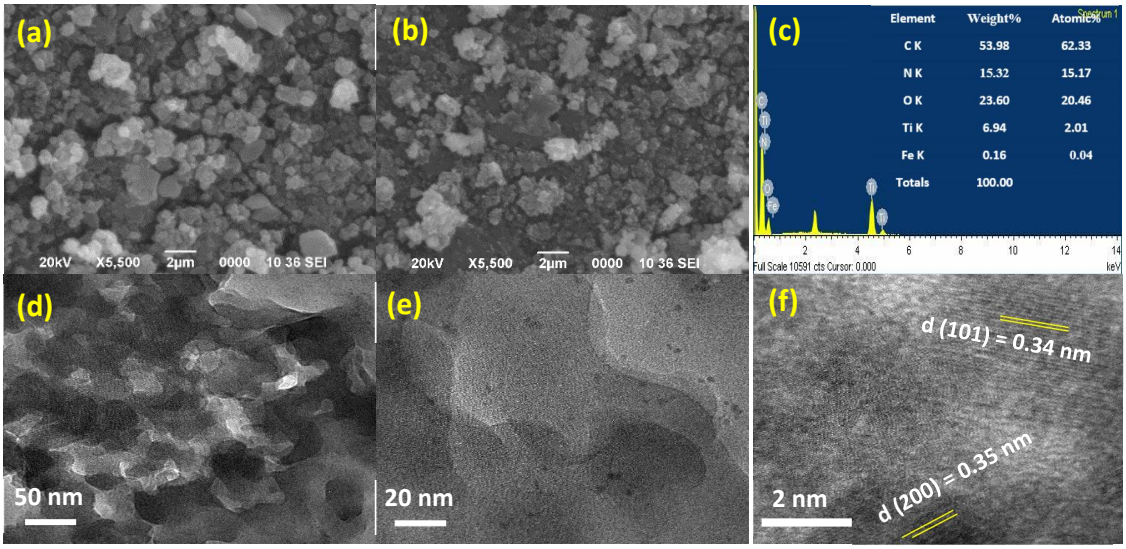

Figure 4.3 SEM images of (a) pure PANI, (b) Fe doped TiO_2@PANI, (c) EDX spectra of Fe doped TiO_2@PANI, (d, e) TEM images of Fe doped TiO_2@PANI at various resolutions shows distribution of Fe doped TiO_2 nanoparticles on PANI, (f) HRTEM of Fe doped TiO_2@PANI with lattice fringes corresponding to d (101) plane and d (200) planes.

SEM image of Fe doped TiO_2@PANI shows rough surfaces compared to that of PANI (**Figure 4.3(b)**). However, no major change has been observed implying that the major component is PANI. EDX analysis suggests the presence of C, N, O, Ti, Fe elements in the expected ratios with negligible impurities (**Figure 4.3(c)**). In **Figure 4.3(d)** and **(e)** the TEM images show nearly homogeneous dispersion of metal oxide nanoparticles on PANI without any agglomeration. HRTEM image **Figure 4.3(f)** exhibits the separation of lattice fringes by 0.35 nm that corresponds to (002) plane of PANI and a d spacing of 0.34 nm, corresponding to significant (101) crystal plane of anatase phase which is in well agreement with the p-XRD data (**Figure 4.1(b)**) and verifies that Fe doped TiO_2 particles are well supported on PANI.

4.3.4 XPS analysis:

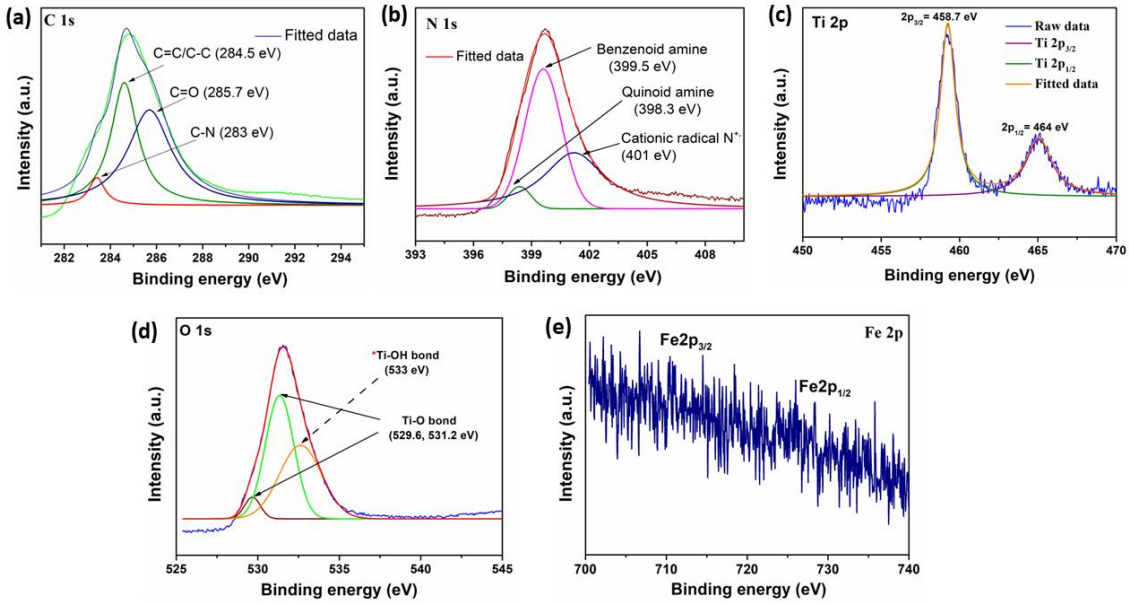

Figure 4.4 High-resolution XPS spectra of Fe doped TiO_2@PANI (a) C 1s, (b) N 1s, (c) Ti 2p, (d) O 1s and (e) Fe 2p.

The elemental valence state and the surface chemical composition of Fe doped TiO_2@PANI catalyst was characterized by XPS analysis. Upon linear fitting the high-resolution spectrum of C (**Figure 4.4(a)**) assigns three distinguished peaks at its 1s orbit at 283 eV which corresponds to C-N functional group, other two peaks at 284.5eV and 285.7 eV ascribed to the C-C/ C=C functional groups and C=O group which results from the surface oxidation respectively. Linear fitting of N 1s spectra manifested three significant peaks indicating the presence of nitrogen in three different states the the benzenoid amine at 399.5 eV, quinoid amine at 398.3 eV, and the cationic nitrogen radical ($N^{+\bullet}$) at 401 eV (**Figure 4.4(b)**). **Figure 4.4(c)** signifies the splitting of the Ti 2p spectrum into two characteristic bands i.e., Ti $2p_{3/2}$ and Ti $2p_{1/2}$ because of the oxidized Ti^{4+} species [13]. The spectrum confirms that Fe doping did not affect the binding energy of TiO_2. O 1s spectrum displays two distinguished peaks at 529.6 eV and 531.2 eV which are responsible for Ti-O bond along with another peak at 533 eV because of the presence of different surface species including hydroxyls, and chemisorbed oxygen (**Figure 4.4(d)**) [20]. In **Figure 4.4(e)** two weak peaks were noticed for Fe 2p spectra verifying Ti–O–Fe bonds as a result of the substitution of Ti^{4+} by Fe^{3+} [13].

4.3.5 Electrocatalytic activity towards HER:

Hydrogen evolution activity of Fe doped TiO_2@PANI composite was examined using a three-electrode set-up in 0.5 M H_2SO_4 electrolyte at ambient temperature. The polarization curves (J-V plots) obtained from linear sweep voltammetry (LSV) measurements with a scan rate of 50 mV sec^{-1} were used to determine the catalytic activity. In this study, all the potentials were calibrated with silver/silver chloride electrode (Ag/AgCl) and then converted to a reversible hydrogen electrode (RHE) using the equation, E (RHE) = E(AgCl) + 0.1976 V.

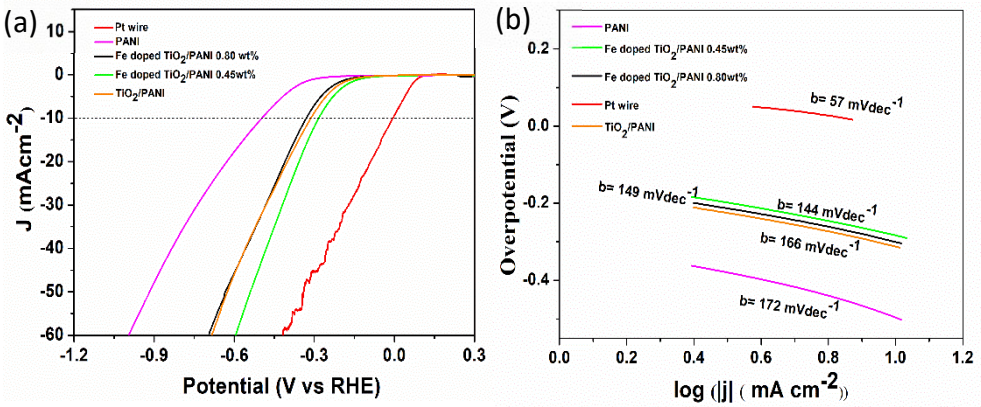

Figure 4.5 Electrocatalytic performance of various catalysts (a) Polarization curves showing onset potentials for HER (b) Tafel plots.

From the non-zero cathodic current measurements Fig. 5. (a), the onset potential for Fe doped TiO_2@PANI with 0.45 wt% was calculated as -0.180 V which is noticeably better than that of TiO_2@PANI (-0.207 V), Fe doped TiO_2@PANI with 0.80 wt% (-0.227 V) and PANI (-0.360 V) with same catalyst loading. It is observed that Fe doped TiO_2@PANI with 0.45 wt% requires a relatively smaller overpotential (η_{10}) of -0.285V vs RHE to obtain the benchmark current density of 10 mA cm^{-2} compared to that of TiO_2@PANI (-0.311 V), Fe doped TiO_2@PANI with 0.80 wt% (-0.331 V) and PANI (-0.498 V). This boost comes from the strong contact of the Fe doped TiO_2 particles with the PANI. DFT study reveals that the interaction of N sites of the PANI with metal oxides substrate leads to a favorable electronic structure that reduces the activation energy for HER on PANI [21]. As we have mentioned earlier a suitable HER catalyst is expected to have H* adsorption-free energy (ΔG_H*) close-to-zero value [22]. Negative ΔG_H value signifies a very strong binding towards the atomic

hydrogen, while positive ΔG_H weakens the interaction of the adsorbed hydrogen on the catalyst surface where both the case impedes the HER kinetics. Thus, unless there is a proper balance between these two conditions the reaction becomes slow. Projected density of states (DOS) study confirmed that PANI has a ΔG_H^* of −1.47 eV, implying a strong H_{ads} interaction on N site of PANI [21]. Thus, desorption of adsorbed hydrogen becomes tough and HER kinetics turn out to be slow. But upon incorporation of metal oxide nanoparticles in PANI there occurs electron transfer from metal atom to N atom of PANI leads the incoming electrons to be filled in the antibonding states of N and thus decreases binding energy of hydrogen with N atom enhancing the HER kinetics. Dopant Fe modifies the electronic structure of TiO_2 by developing new electronic states within the wide band gap of TiO_2. Thus, the electrons from Fe doped TiO_2 easily reach the surface-active sites upon inducing relatively low electric potential to impel HER efficiently. However, upon increasing PANI content after 0.45 wt% the composite efficiency towards HER was found to be decreased. This may be due to the increased PANI content covering the active sites and thus deteriorating catalytic activity.

The kinetics and the mechanistic pathway of HER were analyzed by Tafel slopes, an inherent characteristic of the catalysts. Fe doped TiO_2@PANI shows a small Tafel slope value of 144 mV dec^{-1} (Fig. 5. (b)). A smaller Tafel slope suggests a quicker HER kinetics and a smaller energy requirement for HER.

Electrocatalytic HER proceeds *via* two possible routes:

1) The adsorption reaction with the Tafel slope closer to 120 mV dec^{-1} i.e., Volmer step.

$$H^+ + e^- \rightarrow H_{ads} \qquad \textbf{equation 3}$$

And

2) either of the following routes

a) The electrochemical desorption reaction (Heyrovsky step).

$$H_{ads} + H^+ + e^- \rightarrow H_2 \qquad \textbf{equation 4 (a)}$$

Or

b) The chemical desorption and recombination reaction (Tafel step).

$H_{ads} + H_{ads} \rightarrow H_2$ **equation 4 (b)**

Combination of two of these steps as Volmer-Heyrovsky **equation 3** with **equation 4 (a)** or Volmer-Tafel **equation 3** with **equation 4 (b)** mechanism led to the formation of molecular hydrogen [23]. Tafel slope analysis here ensures that the HER kinetics is likely proceeded by Volmer-Heyrovsky mechanism and releasing of protons on the electrode is the rate determining step. The plausible mechanism on Fe doped TiO_2/PANI is as follows:

$H_3O^+(aq) + e^- + N^* \rightarrow NH_{ads} + H_2O$ (Volmer step)

$NH_{ads} + H_3O^+(aq) + e^- \rightarrow H_2(g) + H_2O(l) + N^*$ (Heyrovsky step)

N* represents the active nitrogen sites of PANI and H_{ads} represents the adsorbed hydrogen.

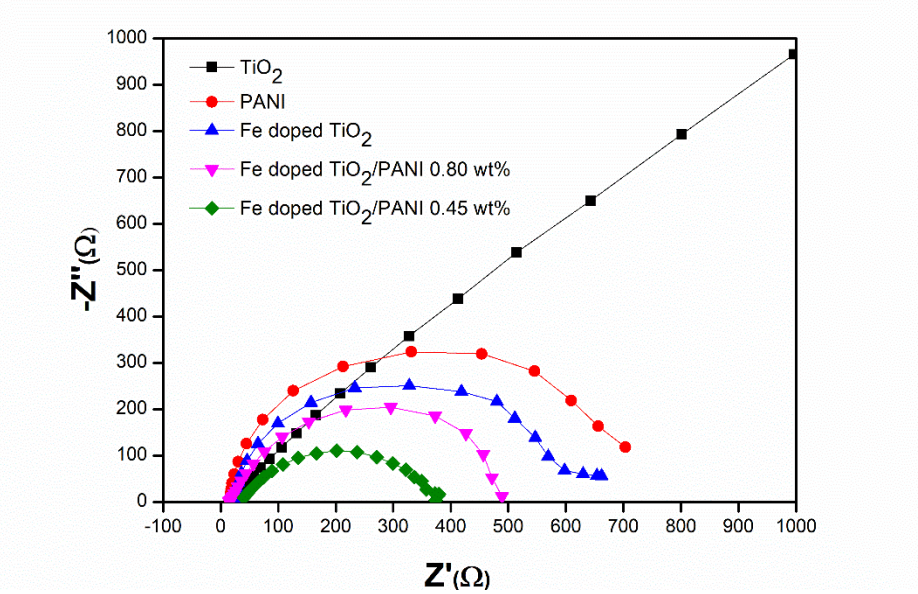

Figure 4.6 Nyquist plots of various synthesized materials

To study the charge transfer resistance between the electrode-electrolyte interface, electrochemical impedance spectroscopy (EIS) analysis was conducted at a fixed overpotential of -270 mV vs RHE within the frequency window of 100 mHz-10 kHz. The charge-transfer resistance (R_{ct}) values deduced from the EIS plots (**Figure**

4.6) are ~6500 Ω, 753 Ω, 588 Ω, 469 Ω, and 335 Ω for TiO_2, PANI, Fe doped TiO_2, Fe doped TiO_2@PANI (0.8 wt%), and Fe doped TiO_2@PANI (0.45 wt%) respectively. A smaller diameter suggests a quicker charge transfer process meaning better conductivity. The smaller R_{ct} value of Fe doped TiO_2@PANI (0.45 wt%), mainly due to the efficient electron transfer from the electrode to the electrolyte suggests the better conductivity of the catalyst validating its faster HER kinetics [24].

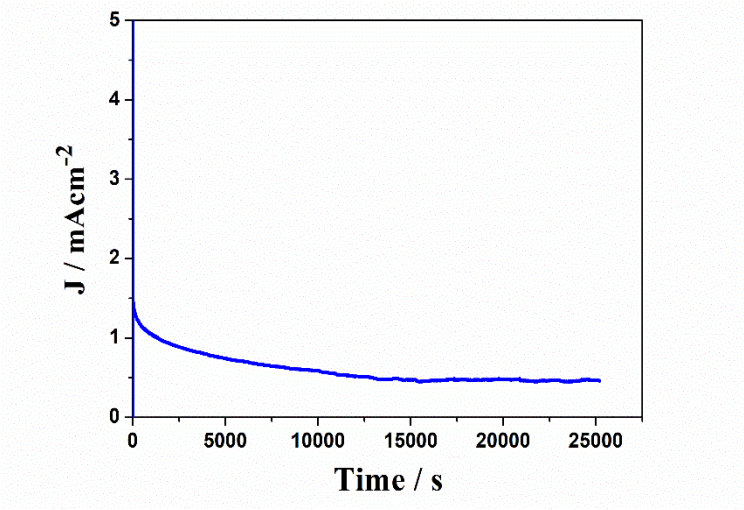

Figure 4.7 Time dependence study of the catalyst Fe doped TiO_2@PANI at an overpotential of -200 mV (Vs RHE) in 0.5 M H_2SO_4

Durability of the catalyst was checked by performing chronoamperometric (CA) analysis for ~7 h at -200 mV (vs RHE) overpotential (**Figure 4.7**). The analysis graph fluctuated due to dehydrogenation via bubble generation and restore of current density after bubble detachment process but the catalyst maintained its integrity in catalytic efficiency towards the end. The durability test represents the applicability of the composite in HER in the acidic medium for a long period.

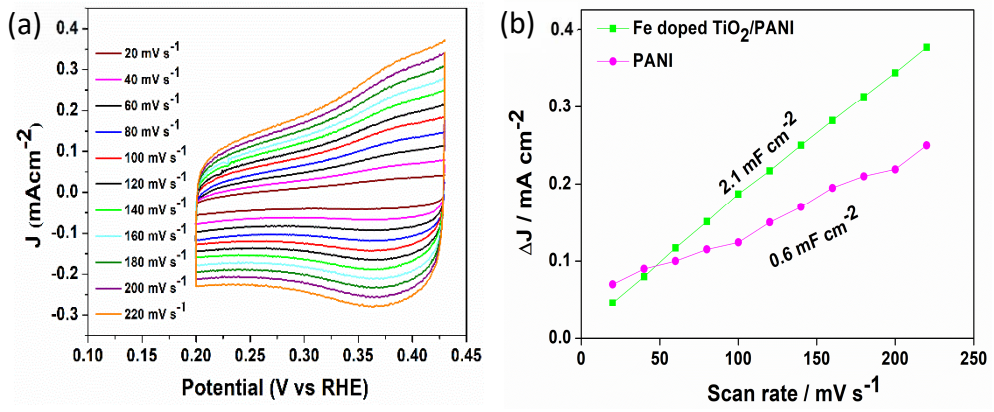

Figure 4.8 (a) cyclic voltammograms at various scan rates from 20 mV s^{-1} to 220 mV s^{-1} within a non-faradic region, (b) variation of capacitive current density against scan rate (C_{dl} values calculated for PANI and Fe doped TiO_2@PANI).

Regarding the remarkable catalytic performance of Fe doped TiO_2@PANI, the voltammetric analysis was performed between the potential of +0.2V to +0.43V with different scan rates where no faradic reaction occurred to discern the electrochemical active surface area (ECSA) (**Figure 4.8 (a)**). Higher ECSA value signifies more catalytically active sites. ECSA was calculated from the electrochemical double-layer capacitance (C_{dl}) that was obtained by fitting the values of the capacitive current (i) and scanning rate (ν) in equation 2.5 [25, 26]. Calculated C_{dl}, R_f *and ECSA* values for the catalysts are given in **Table 4.1**. PANI has a specific role in the homogeneous distribution of Fe doped TiO_2 nanoparticles and thus increases surface active sites for better HER [12]. From these values, it can be proposed that Fe doped TiO_2@PANI even has an advantage in active surface area (ECSA) and active sites over PANI in the improvement of electrocatalytic HER activity.

Table 4.1 C_{dl}, R_f and **ECSA** values obtained for PANI and Fe doped TiO_2/PANI

Working electrode	C_{dl} **(mF cm^{-2})**	R_f **(cm^{-2})**	*ECSA* **(cm^2)**
PANI	0.6	30	2.1
Fe doped TiO_2/PANI	2.1	105	7.35

4.4 Conclusions

This study presents a successful application of environmentally friendly and cost-effective catalyst Fe doped TiO_2@PANI towards HER synthesized via a green method. The composite requires a comparatively small onset potential of 0.180 V than that of PANI (0.360 V). We have tried to turn the PANI surface active towards HER via interfacial electronic interaction with Fe doped TiO_2. The efficiency improvement is solely attributed to the occupancy of the antibonding states that leads to a poor interaction between the adsorbed hydrogen and the catalyst surface. However, better conductivity and improved surface area due to PANI are other factors for better catalytic performance.

4.5 References

[1] Geng, S., Liu, Y., Yu, Y.S., Yang, W., and Li, H. Engineering defects and adjusting electronic structure on S doped MoO_2 nanosheets toward highly active hydrogen evolution reaction. *Nano Research*, *13*:121-126, 2020.

[2] Swaminathan, J., Subbiah, R., and Singaram, V. Defect-Rich Metallic Titania ($TiO_{1.23}$)□ An Efficient Hydrogen Evolution Catalyst for Electrochemical Water Splitting. *ACS Catalysis*, *6*(4):2222-2229, 2016.

[3] Li, S., Yang, H., Ren, R., Ma, J., Jin, J., and Ma, J. Facile fabrication of palladium-ionic liquids-nitrogen-doped graphene nanocomposites as enhanced electro-catalyst for ethanol oxidation. *Journal of Power Sources*, *294*:360-368, 2015.

[4] Román-Martínez, M.C., Cazorla-Amorós, D., Linares-Solano, A., Salinas-Martí'nez De Lecea, C., Yamashita, H., and Anpo, M. Metal-support interaction in Pt/C catalysts. Influence of the support surface chemistry and the metal precursor. *Carbon*, *33*(1):3-13, 1995.

[5] Challagulla, S., Nagarjuna, R., Ganesan, R., and Roy, S. TiO_2 synthesized by various routes and its role on environmental remediation and alternate energy production. *Nano-Structures & Nano-Objects*, *12*:147-156, 2017.

[6] Deng, J., Ren, P., Deng, D., Yu, L., Yang, F., and Bao, X. Highly active and durable non-precious-metal catalysts encapsulated in carbon nanotubes for hydrogen evolution reaction. *Energy & Environmental Science*, *7*(6):1919-1923, 2014.

[7] Chen, S., Wei, Z., Qi, X., Dong, L., Guo, Y.G., Wan, L., Shao, Z., and Li, L. Nanostructured polyaniline-decorated Pt/C@ PANI core–shell catalyst with enhanced durability and activity. *Journal of the American Chemical Society*, *134*(32):13252-13255, 2012.

[8] Roy, S., Payra, S., Challagulla, S., Arora, R., Roy, S., and Chakraborty, C. Enhanced photoinduced electrocatalytic oxidation of methanol using Pt nanoparticle-decorated TiO_2–polyaniline ternary nanofibers. *ACS omega*, *3*(12):17778-17788, 2018.

[9] Voiry, D., Fullon, R., Yang, J., de Carvalho Castro e Silva, C., Kappera, R., Bozkurt, I., Kaplan, D., Lagos, M.J., Batson, P.E., Gupta, G., and Mohite, A.D. The role of electronic coupling between substrate and 2D MoS_2 nanosheets in electrocatalytic production of hydrogen. *Nature materials*, *15*(9):1003-1009, 2016.

[10] Deng, J., Deng, D., and Bao, X. Robust catalysis on 2D materials encapsulating metals: concept, application, and perspective. *Advanced Materials*, *29*(43):1606967, 2017.

[11] Patle, L.B., Labhane, P.K., Huse, V.R., Gaikwad, K.D., and Chaudhari, A.L. Synthesis and structural analysis of Fe doped TiO_2 nanoparticles using Williamson Hall and Scherer Model. *AIP Conference Proceedings*, 1953:030045, 2018.

[12] Huang, Z., Liu, E., Shen, H., Xiang, X., Tian, Y., Xiao, C., and Mao, Z. Preparation of polyaniline nanotubes by a template-free self-assembly method. *Materials Letters*, *65*(13):2015-2018, 2011.

[13] Koli, V.B., Delekar, S.D., and Pawar, S.H. Photoinactivation of bacteria by using Fe-doped TiO_2-MWCNTs nanocomposites. *Journal of Materials Science: Materials in Medicine*, *27*:1-10, 2016.

[14] Zhang, Y., Liu, J., Zhang, Y., Liu, J., and Duan, Y. Facile synthesis of hierarchical nanocomposites of aligned polyaniline nanorods on reduced graphene oxide nanosheets for microwave absorbing materials. *RSC advances*, *7*(85):54031-54038, 2017.

[15] Butoi, B., Groza, A., Dinca, P., Balan, A., and Barna, V. Morphological and structural analysis of polyaniline and poly (o-anisidine) layers generated in a DC glow discharge plasma by using an oblique angle electrode deposition configuration. *Polymers*, *9*(12):732, 2017.

[16] Jarad, A.N., Ibrahim, K., and Ahmed, N.M. Synthesis and characterization thin films of conductive polymer (PANI) for optoelectronic device application. *AIP Conference Proceedings*,1733:020020, 2016.

[17] Tamirisa, P.A., Liddell, K.C., Pedrow, P.D., and Osman, M.A. Pulsed-plasma-polymerized aniline thin films. *Journal of applied polymer science*, *93*(3):1317-1325, 2004.

[18] Ohsaka, T., Ohnuki, Y., Oyama, N., Katagiri, G., and Kamisako, K. IR absorption spectroscopic identification of electroactive and electroinactive polyaniline films prepared by the electrochemical polymerization of aniline. *Journal of electroanalytical chemistry and interfacial electrochemistry*, *161*(2):399-405, 1984.

[19] Singh, T., Pal, D.B., Bhatiya, A.K., Mishra, P.K., Hashem, A., Alqarawi, A.A., AbdAllah, E.F., Gupta, V.K., and Srivastava, N. Integrated process approach for degradation of p-cresol pollutant under photocatalytic reactor using activated carbon/TiO_2 nanocomposite: application in wastewater treatment. *Environmental Science and Pollution Research*, *29*(41):61811-61820, 2022.

[20] Ahuja, P., Ujjain, S.K., Arora, I., and Samim, M. Hierarchically grown NiO-decorated polyaniline-reduced graphene oxide composite for ultrafast sunlight-driven photocatalysis. *ACS omega*, *3*(7):7846-7855, 2018.

[21] Huang, Z.F., Song, J., Du, Y., Dou, S., Sun, L., Chen, W., Yuan, K., Dai, Z., and Wang, X. Optimizing interfacial electronic coupling with metal oxide to activate inert polyaniline for superior electrocatalytic hydrogen generation. *Carbon Energy*, *1*(1):77-84, 2019.

[22] Ji, X., Wang, K., Zhang, Y., Sun, H., Zhang, Y., Ma, T., Ma, Z., Hu, P., and Qiu, Y. MoC based Mott–Schottky electrocatalyst for boosting the hydrogen evolution reaction performance. *Sustainable Energy & Fuels*, *4*(1):407-416, 2020.

[23] Zhu, J., Hu, L., Zhao, P., Lee, L.Y.S., and Wong, K.Y. Recent advances in electrocatalytic hydrogen evolution using nanoparticles. *Chemical reviews*, *120*(2):851-918, 2019.

[24] Zhang, X., Jia, F., and Song, S. Recent advances in structural engineering of molybdenum disulfide for electrocatalytic hydrogen evolution reaction. *Chemical Engineering Journal*, *405*:127013, 2021.

[25] Fang, M., Gao, W., Dong, G., Xia, Z., Yip, S., Qin, Y., Qu, Y., and Ho, J.C. Hierarchical NiMo-based 3D electrocatalysts for highly-efficient hydrogen evolution in alkaline conditions. *Nano Energy*, *27*:247-254, 2016.

[26] Gao, D., Guo, J., Cui, X., Yang, L., Yang, Y., He, H., Xiao, P., and Zhang, Y. Three-dimensional dendritic structures of NiCoMo as efficient electrocatalysts for the hydrogen evolution reaction. *ACS Applied Materials & Interfaces*, *9*(27):22420-22431, 2017.